

Acknowledgments

TransCom is a special project of the IGBP Global Analysis, Interpretation, and Modelling (GAIM) Project. Coordination of the activity was partially funded by the GAIM Office. Additional support for TransCom coordination was provided by the NASA EOS Interdisciplinary Science Program, under contract NAS5-97146.

We thank Pieter Tans and Ed Dlugokencky, who provided the NOAA-CMDL flask data on SF₆, and Dale Hurst, who provided the tall tower time-series data. We are grateful to Sebastian Heimann for assistance in the analysis and graphical display of the time-series data. Computing support for the TM3 simulations has been provided by the Deutsches Klimarechenzentrum (DKRZ), Hamburg. R. Law and P. Rayner were supported by the Australian Government Cooperative Research Centres Programme. I. Fung was supported by the NASA EOS-IDS program and the Canadian Climate Research Network. Jasmin John carried out the computations of the GISS and GISS-UVic model.

Operating funds for the GAIM office have been provided by:

- US National Science Foundation (NSF)
- US National Oceanographic and Atmospheric Administration (NOAA)
- US Department of Energy (DOE)
- US Environmental Protection Agency (EPA)

Overview

The Atmospheric Tracer Transport Model Intercomparison Project (TransCom) is a special project of IGBP/GAIM. The goal is to quantify and diagnose the uncertainty in inversion calculations of the global carbon budget that result from errors in the simulated transport. The specific objectives of the TransCom project are (1) quantify the degree of uncertainty in current carbon budget estimates that results from uncertainty in model transport; (2) identify the specific sources of uncertainties in the models; and (3) identify key areas to focus future transport model development and improvements in the global observing system that will reduce the uncertainty in carbon budget inversion calculations. Our initial intercomparison of global transport models used in the CO₂ inversion problem revealed that inversion estimates of some carbon budget components may currently be uncertain by about a factor of two due to transport alone [Law *et al.*, 1996; Rayner and Law, 1995]. Because the models used in this exercise also form the dynamical core of many models of reactive chemical species, this problem should also be of serious concern to those in the global atmospheric community.

The project is part of a larger GAIM research program which aims to develop coupled ecosystem-atmosphere models that describe time evolution of trace gases with changing climate and changes in anthropogenic forcing. Atmospheric chemical tracer transport models (CTMs) serve three crucial functions in the development, testing, and validation of global Earth system models:

- 1) predictions of trace gas fluxes at the Earth's surface may be used to drive CTMs and the resulting simulations of atmospheric concentrations may be compared to observations to test Earth system models;
- 2) trace gas fluxes at the surface may be calculated from observations of atmospheric concentration "inversion" of the data with a CTM, improving process-level understanding and directly validating Earth system models; and
- 3) simulation of the fate and temporal evolution of reactive trace gases such as methane (CH₄) and nitrous oxide (N₂O) requires a detailed atmospheric chemistry module in Earth system models, which includes both transport and chemical transformation.

An important source of uncertainty in these calculations is the simulated transport itself, which varies among the many transport models used by the community. TransCom investigators have conducted a series of 3-dimensional tracer model intercomparison experiments with leading transport codes which are intended to (1) quantify the degree of uncertainty in current carbon budget estimates that results from uncertainty in model transport; (2) identify the specific sources of uncertainties in the models; and (3) identify key areas to focus future transport model development and improvements in the global observing system that will reduce the uncertainty in carbon budget inversion calculations. Results of an initial intercomparison of simulations of fossil fuel CO₂ and the influence of seasonal vegetation were reported by Rayner and Law, [1995] and by Law *et al.*, [1996]. A second phase of TransCom, involving calibration simulations of sulfur hexafluoride (SF₆) has been conducted as well, with results reported by Denning *et al* (1998).

Atmospheric trace gas concentration is affected both by chemical and physical processes. Some trace gases such as methane are chemically reactive in the atmosphere, being lost to oxidation. They are also physically transported so that its atmospheric distribution is not directly related to its ground sources. Both mechanisms must be quantified in order to understand global atmospheric trace gas distribution, but atmospheric trace gas transport codes are highly variable in their results, and need reconciliation. In order to effectively diagnose transport codes, they must be first compared in their prediction of passive trace gases, so that the physical effects can be separated from the chemical. Consequently, we will begin by considering the simpler case of chemically non-reactive CO₂, and as a first step, we will examine some passive tracers which have no sinks so that we can most effectively compare model results and thus promote model refinement. We will treat the methane budget separately (described below), in preparation for ultimately incorporating atmospherically reactive methane into the demonstrably realistic transport codes developed in association with the transport component of the project.

Phase 1 of TransCom involved simulation of the response of atmospheric CO₂ to anthropogenic emissions and to seasonal exchange with the terrestrial biosphere. Intercomparison of about a dozen such simulations showed a surprising degree of

variability, even in the annual mean north-south gradient. Many of the same models are also used for investigation of the distribution of reactive species such as CH₄, so significant disagreement on CO₂ distribution is unsettling since the transport of a passive tracer should be relatively easy to simulate. The models behaved similarly for the fossil fuel experiment, with most simulating about 4 ppm difference between the Arctic and the Antarctic, although there were outliers that led to an overall distribution of about a factor of two. This relative consensus was not present aloft, with qualitative disagreement among the models in the middle and upper troposphere. The simulated response to purely seasonal exchange with plants and soils was reasonably successful at capturing the observed seasonal amplitude. However, consistent phase errors among the models suggested that a previously published estimate of terrestrial CO₂ exchange fails to properly represent the boreal spring uptake. In the annual mean, some models produced a strong north-south gradient due to these purely seasonal exchanges due to interactions between the terrestrial flux and the simulated atmospheric transport. Unfortunately, these experiments did not include a complete carbon budget (no air-sea fluxes were prescribed, for example), so a direct comparison to observations was not possible. An additional set of experiments was planned for "calibration" of the models against a trace gas for which adequate data could be used to determine which simulations were in error.

Phase 2 of TransCom involved intercomparison of the distribution of SF₆, which has very slowly varying sources, no sinks, and is reasonably well observed around the globe. The results of this experiment showed that most of the models agree quite well with the data at the surface in remote marine locations, with the degree of consensus decreasing in continental interiors and aloft where data coverage is poor. Those models which were most successful at reproducing the observed north-south gradient in remote marine locations systematically overestimated SF₆ levels near source regions, and vice versa. This experiment included much more detailed diagnostics of the mechanisms by which the models transported the tracer. A significant finding was that the north-south gradient *at the surface* is primarily controlled not by interhemispheric mixing, but rather by *vertical* mixing, which occurs at unresolved spatial scales and must be parameterized in the models. Interhemispheric transport in most models was dominated by resolved advection, with a minority of the codes relying more on parameterized diffusion to achieve missing into the southern hemisphere. In general, differences among the models were explained to a large degree by differences in the subgrid-scale parameterized transport rather than by differences in numerical advection schemes or differences in spatial resolution. Analysis of the results of this experiment is continuing.

A third phase of the TransCom project is currently being planned, and will involve an intercomparison of inversion calculations of the atmospheric CO₂ budget. The models will be used to simulate the atmospheric response to an agreed-upon set of surface emission "basis functions" representing regional emissions and uptake of CO₂ due to various processes (industrial emissions, ecosystem metabolism, air-sea gas exchange, biomass burning, etc). The focus of this inversion intercomparison activity will be to produce a formal estimate of the degree of uncertainty in such an inversion calculation that arises directly from the uncertainty in the model transport as represented by the population of participating models. It is hoped that this ambitious activity can begin in late 1998, and that it can be completed in 2000-2001. A final phase of the project will use a set of sensitivity experiments to isolate the components of the models that are most responsible for the different behavior they exhibit, using the results to recommend priorities for future model development to reduce uncertainty.

Motivation

A key component in the projection of future global change is the ability to predict future concentrations of atmospheric greenhouse gases such as carbon dioxide (CO₂) and methane (CH₄). Unfortunately, the current state of the science cannot completely account for the growth rate and interannual variations of atmospheric CO₂ and CH₄ with confidence, so accurate prediction of future concentrations is difficult. One of the objectives of GAIM is to develop coupled ecosystem-atmosphere models that describe time evolution of trace gases with changing climate and changes in anthropogenic forcing. Such a coupled Earth system model must include an atmospheric module which adequately describes the chemical transformations with the atmosphere, and biospheric modules which describe the emissions from different ecosystems as well as how the emissions react to climate changes. The models must be based on process-level understanding of trace gas exchanges and transformations, but can be constrained by trace gas concentrations measured by the global observing network.

Only about half of the anthropogenic CO₂ remains in the atmosphere, and the fate of the other half is not completely understood. Both the ocean and terrestrial biosphere currently act as significant sinks for anthropogenic CO₂, but their relative contributions are a matter of intense debate [Houghton *et al.*, 1995]. The terrestrial net sink is very difficult to measure directly, even at a single location, because it results from a small imbalance between large natural uptake and efflux by photosynthesis and ecosystem respiration, neither of which can be accurately measured at large spatial scales. Until the mechanisms involved in the terrestrial uptake are more clearly elucidated, predicting the future behavior of such a sink (and therefore the atmospheric concentration) will be very difficult. A significant step toward this end was taken in the recent GCTE synthesis [IGBP, 1997].

The spatial and temporal distribution of atmospheric trace gas concentrations contains a great deal of information about the distribution of sources and sinks at the surface (e.g., [Conway *et al.*, 1994; Francey *et al.*, 1995; Keeling *et al.*, 1995]). This information is key to the overall effort to understand ecosystem-atmosphere interactions because (1) the concentration field provides validation data for the testing of coupled ecosystem-atmosphere models (a "bottom-up" approach to the problem); and (2) careful analysis of the changing distribution of trace gases can yield estimates of surface fluxes on the largest spatial scales (a "top-down" or "inverse" approach). Direct observation of trace gas concentrations through flask sampling and aircraft campaigns provides the data for these calculations, but calculation of surface emissions and uptake requires a detailed understanding of the atmospheric transport and chemical transformation that occur prior to samples being collected. This requires a numerical simulation model of scalar tracer transport by the atmosphere, which may be driven by analyzed winds or from meteorological principles, and may include gas transport, reactive chemistry, or both. The "top-down" or "inversion" approach has long been used to study sources and sinks of atmospheric CO₂ [Ciais *et al.*, 1995; Enting and Mansbridge, 1989; Enting and Mansbridge, 1991; Enting *et al.*, 1995; Fung *et al.*, 1983; Heimann and Keeling, 1989; Tans *et al.*, 1989; Tans *et al.*, 1990]. It has also been used to study atmospheric CH₄ [Fung *et al.*, 1991], chlorofluorocarbons [Hartley and Prinn, 1993; Prather *et al.*, 1987], and many other trace gases, both reactive and inert.

As high time-resolution global data on additional species become available ($\delta^{13}\text{C}$ and $\delta^{18}\text{O}$ of atmospheric CO₂ and atmospheric O₂/N₂ ratio), the use of synthesis inversion techniques with atmospheric tracer transport models will result in much more reliable estimates of the changing global carbon budget of the atmosphere. Improvements in the quality and quantity of the observational data and in the mathematical formalism associated with the inversion calculation have brought us to the point where one of the greatest sources of uncertainty now lies in the transport models themselves.

Simulations of the distribution of reactive species are being evaluated through several other programs (IGAC-GIM, WMO, WCRP, etc.). In these activities, models differ both in terms of scalar transport and reactive chemistry, complicating accurate diagnosis of the mechanisms producing the differences among the results. Previous model intercomparison studies have also addressed the transport of passive tracers such as CFC-11 [Prather, 1996] and ²²²Rn [Jacob *et al.*, 1997]. TransCom has focused instead on the CO₂ problem for several reasons:

- 1) CO₂ is the primary anthropogenic greenhouse gas;
- 2) It is nonreactive, so that differences in model simulations can be understood in terms of differences in transport rather than some combination of transport, reactive chemistry, or interactions among these;
- 3) Unlike CFCs, ²²²Rn, or other previously studied passive tracers, the surface exchange of CO₂ has a very strong seasonal and diurnal cycle which is superimposed on the relatively weak anthropogenic emissions and natural sinks; and
- 4) The biological processes which control natural CO₂ exchange at the land surface also affect atmospheric circulation, which may complicate the interpretation of spatial distribution measured by field sampling [Denning and Randall, 1995].

The first set of experiments performed by TransCom investigators [Law *et al.*, 1996; Rayner and Law, 1995] involved the effects of transport on anthropogenic emissions of CO₂ due to fossil fuel combustion, which is strongly concentrated in the northern hemisphere and were assumed to have no temporal variations, and exchange with terrestrial ecosystems which have very strong seasonality but were assumed to have no annual net source or sink at any location. This approach allowed

an evaluation of the different model formulations with respect to interhemispheric exchange (of the fossil fuel tracer), the amplitude of the seasonal cycle (of the biosphere tracer), and covariance between surface flux and atmospheric transport of the biosphere tracer. Unfortunately, it is impossible to observe the atmospheric concentrations of CO₂ specifically related to either fossil fuel emissions or exchange with terrestrial ecosystems. So although these experiments exhibited a surprising degree of model-to-model differences, it is impossible to rate the various simulations in absolute terms of agreement with the real atmosphere.

To "calibrate" the performance of the various models with respect to interhemispheric gradients of passive tracers, we needed to move beyond the simulations of unobserved (and unobservable) fossil fuel CO₂ to a tracer that was well observed and whose atmospheric budget was not complicated by missing sinks. This requires a tracer with well-documented concentrations around the world, with a quantifiable emissions field, and preferably with insignificant sinks. Previous studies have used CFCs for this purpose, but since the Montreal Protocols were implemented, the emissions of CFCs have been declining so rapidly that the concentration field has been out of equilibrium with the emissions field, making the observations difficult to interpret. Instead, we chose to calibrate the models by simulating the distribution of sulfur hexafluoride (SF₆), a nonreactive anthropogenic tracer which is released primarily from electrical distribution equipment [Maiss *et al.*, 1996]. The advantages of SF₆ are that it has no sinks and therefore has a smoothly increasing time series which is easy to interpret, and that it is now measured at a relatively large number of stations around the world [Crutzen *et al.*, 1998; Geller *et al.*, 1997; Maiss *et al.*, 1996]. Because the emissions and concentration field for SF₆ are much better known than for CO₂, we have been able to use the results of this calibration experiment to evaluate the realism of the large-scale interhemispheric transport characteristics of each model in a context for which we know the "right answer." In addition, the calibration experiment included the calculation of transport diagnostics designed to help elucidate the mechanisms by which the various models produce their different tracer distributions. We hope that the results of the intercomparison and calibration phases of the project can be used to diagnose problems with the existing transport codes.

The next phase of the project will involve intercomparison of inversion calculations of the carbon budget of the atmosphere, with the objective of quantifying the uncertainty in such calculations that arises directly from uncertainty in the simulated transport. Finally, we will perform a set of sensitivity experiments and conduct a detailed diagnosis of the various components of the transport (resolved advection, cumulus convection, diffusion, etc.), to identify the mechanisms that lead to discrepancies between the models and the observations. Each modelling group is expected to use the results of these experiments to improve their codes. Computation of the contemporary carbon budget of the atmosphere using the suite of calibrated and improved models will provide both more reliable estimates of the terrestrial sink and (more importantly) a better set of tracer transport models for future research.

Participating Models:

Twelve modelling groups submitted results for Phase 1 of the project. Ten groups submitted results for the SF₆ experiment, including most of the participants in the TransCom 1 intercomparison as well as several additional models (Table 1). "On-line" models, (CCC, CSU, and GFDL-SKYHI) simulate tracer transport in a fully prognostic general circulation model (GCM), calculating winds and subgrid-scale transport on time steps of minutes. "Off-line" models (CTMs) calculate tracer transport from either analyzed winds (NIRE, TM2) or GCM output (GFDL-GCTM, GISS, GISS-UVic, MUTM, TM3). The off-line models are able to use much longer time steps, and specify input wind fields with frequencies varying from 1 hour to 1 day. Subgrid-scale vertical transport was parameterized in all models, using a variety of techniques. Off-line models generally include schemes to calculate these terms from the prescribed wind input, whereas online models calculate subgrid-scale transports at the same time as the dynamical calculation of the GCM winds. GCM calculations used on-line winds calculated using climatological sea-surface temperatures as a lower boundary condition. Each model is described in more detail in Appendix A.

Table 1: Participating Models

Model	Contact	Type	Reference	Horizontal Grid	# Levels	Advection	Wind	Freq	Parameterized Transport			
									H Diff	Y Diff	Conv	Explicit PBL
CCC	Holzer	GCM	McFarlane <i>et al</i> , 1992	3.75°	10 sigma/pres	Spectral	On-line	-	Y	Y	B	N
CSU	Denning	GCM	Denning <i>et al</i> , 1996	4° x 5°	17 sigma	2 ¹⁴ order	On-line	-	N	N	C	Y
GFDL-GCTM	Fan	CTM	Mahlman and Moxim, 1978	256 km	11 sigma	2 ¹⁴ order	GFDL ZODIAC	6 hr	Y	Y	A	N
GFDL-SKYHI	Fan	GCM	Hamilton <i>et al</i> , 1995	3° x 3 . 6°	40 sigma	2 ¹⁴ order (horiz), 4 ¹¹ (vert)	On-line	-	Y	Y	A	N
GISS	Fung	CTM	Hansen <i>et al</i> , 1997	4° x 5°	9 sigma	Slope	GISS GCMII	4 hr	Y	N	B	N
GISS-UVIC	Fung/ Friedlingstein	CTM	Hansen <i>et al</i> , 1997	4° x 5°	9 sigma	Slope	GISS GCMII	1 hr	N	N	C	N
MUTM	Law	CTM	Law <i>et al</i> , 1992	3.3° x 5.63°	9 sigma	Spectral	MU GCM7	24 hr	Y	Y	B	N
NIRE	Taguchi	CTM	Taguchi <i>et al</i> , 1996	2.5°	15 sigma/pres	Semi-lagrangian	ECMWF (93)	6 hr	N	N	N	Y
TM2	Bakanski/ Bousquet	CTM	Bousquet <i>et al</i> , 1996	7.5° x 7.5°	9 sigma	Slope	ECMWF (93)	12 hr	N	Y	C	N
TM3	Heimann	CTM	Heimann, 1995	3.75° x 5°	19 sigma	Slope	ECHAM 3 GCM	6 hr	N	Y	C	N

-Convection Categories:

A. Simple Diffusion

- B. Pairwise layer Mixing
- C. Penetrative Mass Flux

Phase 1 (Meridional Gradients and Seasonal Cycles):

Method

Two sources of CO₂ were chosen for this part of the model intercomparison. The first was the emissions of CO₂ due to fossil fuel burning and cement production. This is one of the best known components of the CO₂ budget and makes a good test of a model's interhemispheric transport since 95% of the fossil fuel emissions occur in the northern hemisphere. The source data used were provided by I. Fung and have been used previously [Tans *et al.*, 1990]. They are based on country estimates [Marland *et al.*, 1989] which have been distributed within countries according to population density. They include no temporal variation. The data were provided on a 1 x 1 degree grid with modelers aggregating this to their own model resolution.

The second source used was the exchange of CO₂ with the biosphere. The data were compiled by combining satellite estimates of photosynthesis with local measurements of respiration and net primary productivity [Fung *et al.*, 1987]. The sources were validated by comparing modeled (using the GISS model) and observed seasonal cycles of CO₂ concentration. This source is the major contributor to the observed seasonal cycle of CO₂, at least in the northern extra-tropics. Thus some comparisons can be made between modeled and observed seasonal cycles. There is also considerable interest in the annual mean CO₂ field which results from the combination of seasonal sources and seasonal variation in transport.

The experiments, referred to here as the fossil and biosphere experiments, were run for at least three years from an initial atmosphere with uniform CO₂. This provides sufficient time for the model atmosphere to establish "equilibrium" (annually repeating) concentration distributions determined by the surface sources. Contributing modellers supplied concentration fields for the surface layer, 500 and 200 mb. In addition, zonal mean cross-sections were analyzed. Each set of results has been normalized such that the January global three-dimensional mean is zero.

Fossil Fuel Experiment

Differences in interhemispheric transport between models can be seen in the zonal annual mean surface concentrations (Figure 1). While each model gives a broadly similar distribution, with maximum concentrations around 50°N and relatively small gradients through the southern hemisphere, there are large differences in the maximum and minimum concentrations. The range of concentrations found for the northern mid-latitudes can be reduced by almost half if the CSIRO9 and GFDL results are excluded. It is likely that this smaller range is more realistic since there have been reported calibrations of meridional mixing using krypton-85 for the GISS and TM1 models [Heimann and Keeling, 1989; Jacob *et al.*, 1987] which lie in this range.

The variation among models can be summarized by the interhemispheric concentration difference (northern minus southern hemisphere mean concentration); listed alongside each model identifier in figure 1. The interhemispheric differences vary by a factor of two. It is important to note that these differences are surface values and the variation between models reflects differences in both vertical and cross-equatorial transport. The CSIRO9 model produces the largest difference (4.7 ppmv) and the MU models the smallest (2.4 ppmv). In order to understand this difference better, MUTM (an offline model) was run with winds taken from the CSIRO9 model. This simulation produced an interhemispheric difference of 3.6 ppmv which indicates that, in this case, the large-scale winds account for about half the difference between the model results with the sub-grid scale parameterizations accounting for the other half.

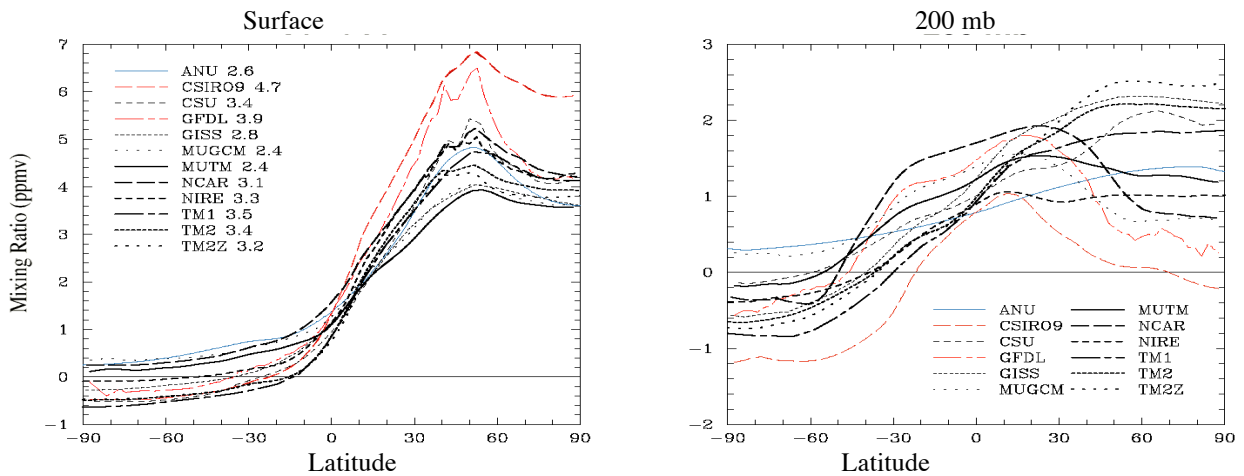


Figure 1: Zonal mean annual mean mixing ratio of CO₂ response to fossil fuel emissions as simulated by 12 tracer transport models. The value at the south pole has been subtracted. The left panel shows the response at the Earth's surface (or in the lowest model layer), and the right panel shows the response at the 200 mb pressure level. Colored lines are used consistently across figures to indicate the CSIRO9, GFDL-GCTM, and ANU models, which behaved differently from the others.

The qualitative agreement in model responses at the surface breaks down at 200 mb (Figure 1b). Approximately half the models produce maximum concentrations around 0°–30°N while the remainder have mid to high northern latitude maxima. The models that produce the highest surface concentrations in the source region (CSIRO9 and GFDL-GCTM, shown in red in Figures 1-3) produce among the lowest values aloft. This suggests that the high surface values may be more closely related to vertical "trapping" of the tracer in the vicinity of strong emissions rather than weak southward transport. The tropical maxima at 200 mb in some simulations probably result from strong cumulus convection whereas minima in higher latitudes reflect weak vertical motion. Nakazawa et al. [Nakazawa et al., 1991] measured CO₂ concentration in the upper troposphere on flights between Tokyo and Sydney (36°N to 30°S) and found maximum annual mean concentrations around 0°–10° N. This would be more consistent with those models that produce low latitude maxima at 200 mb. However, it is important to note that the observed values are for CO₂ from all sources whereas the modeled results are for the fossil source only. Also, the model data at 200 mb may include stratospheric air whereas this has been excluded from the observed data. The ANU model produces a more uniform distribution than the other models. This suggests that there is rapid horizontal mixing acting to reduce the meridional gradient. Weak vertical mixing could also contribute but this is less likely because the ANU 200 mb global mean concentration is similar to those from other models.

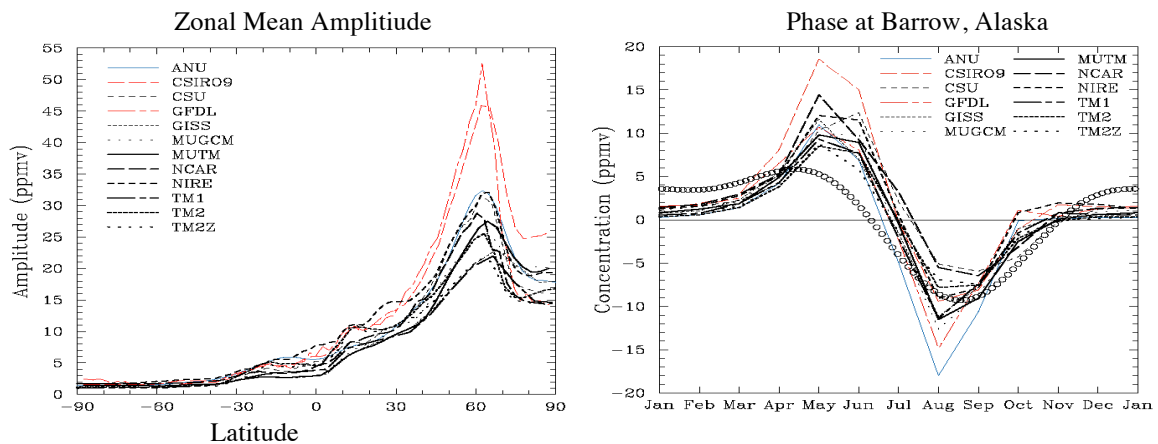


Figure 2: Seasonal cycle of CO₂ response to terrestrial exchange fluxes of *Fung et al.* [1987] simulated by 12 atmospheric tracer transport models. The left panel shows zonal mean annual peak-to-peak amplitude at the surface; right panel shows monthly mean surface values for the grid cell corresponding to Point Barrow, Alaska, with circles indicating the observed seasonal cycle [Conway et al., 1994]. Colored lines indicate CSIRO9, GFDL-GCTM, and ANU models as in Figures 1 and 3.

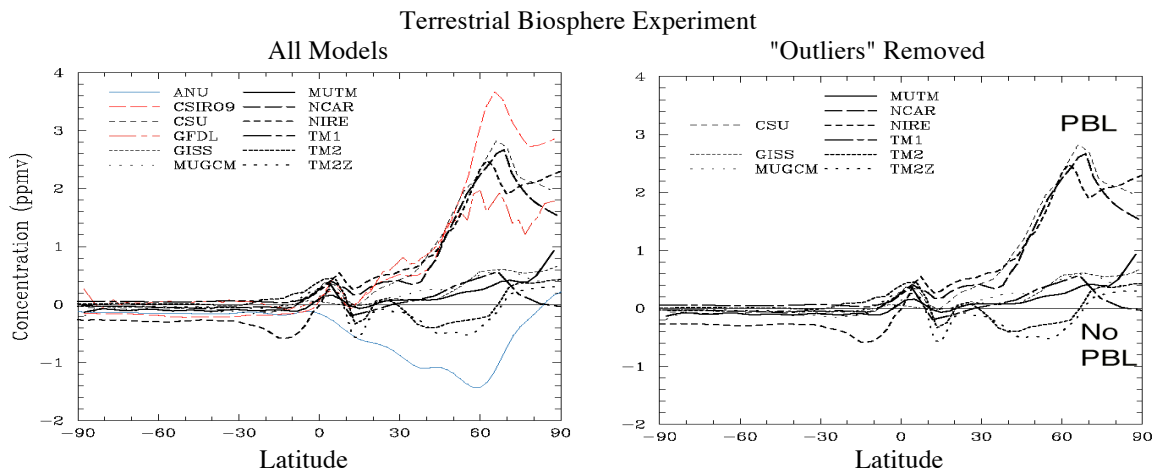


Figure 3: Annual mean zonal mean surface CO₂ mixing ratio response to purely seasonal exchange with the terrestrial biosphere as simulated by 12 atmospheric tracer transport models. The left panel shows all the models, with colored lines indicating the CSIRO9, GFDL-GCTM, and ANU models as in Figures 1 and 2. The right panel is identical except that the "outlier" models have been removed.

Biosphere Experiment

The seasonal nature of the biospheric source provides many options for characterizing the models' responses. We choose here to focus on the amplitude of the seasonal cycle and the surface annual mean response.

The peak to peak (ptp) amplitudes are calculated as the difference between the maximum and minimum monthly mean concentration at each grid point. The zonal mean ptp amplitude at the surface (Figure 2a) increases from around 1–2 ppmv in the southern mid and high latitudes to between 22 and 52 ppmv (32 without CSIRO9 or GFDL) around 65°N. The larger values produced by CSIRO9 and GFDL are probably due to slow mixing out of the surface layer. This interpretation is consistent with the strong meridional gradients produced by these models in the fossil experiment and also with the low

concentrations these models exhibit at 200 mb above the source region. As in the fossil experiment, the results from the CSIRO9 and MU models are very different. We have also performed the biosphere experiment forcing MUTM with the CSIRO9 winds. The ptp amplitudes that result are almost identical to those produced by MUTM (forced with MUGCM winds), particularly in the northern mid and high latitudes. This suggests that the sub-grid scale parameterizations control the amplitude of the seasonal cycles at these latitudes.

The largest range of amplitudes in Figure 2a which occurred at Barrow. Figure 2b shows the surface monthly mean concentration for each model at this site. Also shown is the observed seasonal cycle represented by the first two harmonics fitted to detrended data from *Conway et al.*, [1994]. In general there is close agreement between models in the structure of the seasonal cycle although there are large discrepancies in the magnitudes of the maximum and minimum concentrations. Comparison of the models with the observed seasonal cycle reveals some systematic problems, however. All models produce a maximum value which is too large and occurs too late. The winter concentrations are too low but the August-November period is reasonably simulated. Since all the models are producing similar errors, this suggests an error with the input sources rather than with the model transport, particularly as similar discrepancies are seen at most of the high northern latitude sites. Low light and long atmospheric path lengths result in errors in the NDVI (and hence CO₂ fluxes) at high latitudes in Spring. There may also be errors in the respiration estimates through the use of air temperatures rather than soil temperatures. This illustrates the potential extra information that can be gained by running a range of transport models. Had only one result been available it would be more difficult to distinguish between source and transport errors.

While the annual mean biospheric source is zero everywhere, this is not true of the spatial distribution of annual mean concentration resulting from this source. The interaction of seasonal variations in transport with the seasonal source produces non-zero annual mean concentrations. The zonal annual mean (Figure 3a) shows that for some models (CSIRO9, CSU, GFDL, NCAR and NIRE) the north-south gradient is around half that produced in the fossil experiment. Most models produce small positive concentrations around the equator. These result from the seasonal shift of the ITCZ. The positive concentrations in the northern mid-latitudes appear to be more associated with seasonality in vertical transport. For example, experiments with MUTM have shown that seasonality of convection is important.

The annual mean response of the ANU model is qualitatively different from the other models. Taylor (pers. comm.) has indicated that the negative concentrations result from the use of 1980 winds at only 7 levels; small positive concentrations were obtained in subsequent experiments when winds from the 1990s at 14 or 15 levels were used. When this model (shown in blue in Figures. 1-3) and the CSIRO9 and GFDL-GCTM models (which appear to exhibit unrealistic vertical trapping) are removed (Figure 3b), the remaining results cluster into two populations. Models with explicit formulations of vertical mixing in a variable-depth planetary boundary layer exhibit strongly elevated annual mean surface concentrations over the northern hemisphere, whereas the others do not. It is likely that the seasonality of the PBL depth contributes to the positive annual means due to "rectification" of the seasonal fluxes [Denning *et al.*, 1995; Keeling, 1989; Taguchi, 1996]. The ability to resolve changes in vertical mixing due to the diurnal cycle may also be important [Denning *et al.*, 1996].

Conclusions from Phase 1

We have compared the simulation of CO₂ concentration due to fossil fuel emissions and biospheric exchange by 12 atmospheric tracer transport models. While each model produces broadly similar concentration distributions there is a large range in the efficiency of transport among models. For example, surface interhemispheric exchange times varied by a factor of two, although this range can be significantly reduced by removing a few outlier responses.

The implications of these results for CO₂ budget studies are substantial. In addition to the range in meridional gradient produced by the fossil experiment, there is no clear consensus among models on the annual mean response to the biosphere exchange. The uncertainties in transport produce uncertainties in regional carbon budgets comparable to those from other elements of the inversion. Uncertainties in transport can also be expected to impact modelling of other chemical species in the atmosphere, whenever the lifetime is long enough that transport affects the distribution of the species. More detailed observations of CO₂ and other species, particularly aloft and over the continents, can play a major role in constraining both transport and net sources.

Phase 2 (Calibration and Diagnosis with SF₆):

Sulfur hexafluoride is an anthropogenic trace gas with an atmospheric lifetime of over 3000 years [Ravishankara *et al.*, 1993], whose mixing ratio is increasing rapidly in the troposphere [Geller *et al.*, 1997; Levin and Heshaimer, 1996; Maiss and Levin, 1994; Maiss *et al.*, 1996]. It is believed to be emitted by slow leakage primarily from electrical switching equipment, which is its main industrial use. Its time series is very "clean" and easy to interpret. Unlike other anthropogenic tracers such as CFCs and krypton-85, the growth rate of global emissions is relatively steady, so the annually averaged concentration field is in a quasi-stationary state. The global source has been estimated from the time series of its mixing ratio at various locations using archived air samples [Maiss *et al.*, 1996]. The spatial pattern of SF₆ mole fraction at the surface is reasonably well characterized by a set of flask sampling programs and by intensive sampling programs, and the sampling density is growing rapidly.

Experimental Method

The experiment consisted of integrating each model surface forcing of SF₆ emissions prescribed as closely as possible to the real values, and saving model data corresponding to observations. We also saved a suite of diagnostic fields for comparison from model to model.

Emissions of SF₆ were prescribed according to the global estimates [Levin and Heshaimer, 1996]. These global estimates were linearly interpolated to daily values defined on the fifteenth of each month between December 1988 and January 1994 to avoid "shocks" associated with changing emission rates at year boundaries. The global emissions were distributed geographically on a 0.5° x 0.5° grid, according to electrical power usage by country [United Nations, 1994] and population density [Tobler, 1995]. This distribution reflects the predominant source of SF₆ to the troposphere by leakage from electrical switching equipment. Each participating group then computed the area-weighted average of the emissions distribution onto their (coarser) model grid, and scaled the values to preserve the global integrity.

The models were initialized with a globally uniform tracer distribution for January 1, 1989. An initial condition of 2.06 parts per trillion by volume (pptv) was specified, using the model of Maiss *et al.*, [1996]. Each model then integrated the tracer calculation for 5 years, updating the emissions field daily, ending on December 31, 1993. Results were archived for the final 12 months of the integration, and each group submitted a large set of simulated tracer statistics and transport diagnostics, as described below.

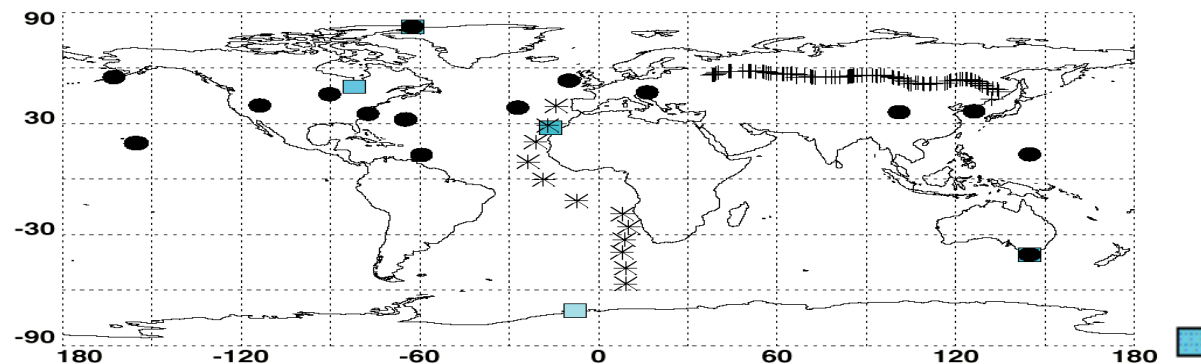
Diagnostic output was designed to provide both an opportunity to compare the simulated SF₆ abundance to observational data, and to elucidate mechanisms for the different behavior of the model simulations. Our experience in TransCom Phase 1 suggested that this would require information about both resolved advective transport and subgrid-scale parameterized transport. Interpolation of transport diagnostics to pressure coordinates and the use of vertically integrated mass transport slabs was intended to allow budgets to be estimated and to allow quantitative comparison of the various components of such budgets. Resolved advection was calculated in terms of mass fluxes, and subgrid-scale parameterized transport was presented as tendencies. Mass fluxes were calculated from "local anomaly" mixing ratios ($C^+ \equiv C - C_0$) after subtracting the global mean (background) mixing ratio of sulfur hexafluoride (C_0), to provide a more robust estimate of the divergence of the advective transport.

Observational data

Observational data used to evaluate model performance were gathered from a number of sources representing various time periods and frequencies (Figure 4). Time series of SF₆ mole fraction from continuous analyzers and archived air samples were available for five stations representing the remote troposphere at latitudes from 83° N to the Antarctic coast over time periods ranging from one to twenty-five years [Levin and Heshaimer, 1996; Maiss *et al.*, 1996]. A meridional profile was obtained from measurements taken during a ship cruise in the Atlantic Ocean during October/November 1993 [Maiss *et al.*, 1996]. Flask samples from a subset of the NOAA-CMDL network have been analyzed for SF₆ since early 1996 (E.

Dlugokenky and P. Tans, personal communication). Hourly time series of SF₆ have been measured along with a suite of other trace gases near the top of tall television towers in North Carolina (WITN-TV) and Wisconsin, USA (WLEF-TV) since 1994 [Hurst *et al.*, 1997]. Two SF₆ transects across Eurasia from Moscow to Vladivostok were measured during

1996 by *Crutzen et al.*, [1997] on the Trans-Siberian Railroad. Many of the observational data have become available since the experimental protocol was developed. The rapid accumulation rate of SF₆ in the troposphere precludes the direct comparison of these data to the model simulations for 1993. Data collected in other years was extrapolated in time to 1993 for comparison to models by one of two methods (Table 2): (1) data from sites with sufficiently long time series were extrapolated using a linear trend determined from the data; and (2) other data were extrapolated using the quadratic fit to the global mean trend suggested by *Maiss et al.*, [1996].



Heidelberg data (Maiss et al, 1996)

* Atlantic Transect, November 1993 (Maiss et al, 1996)

+ Trans-Siberian Railroad Transect (Crutzen et al, 1997)

● NOAA-CMDL Flask Data (E. Dlugokencky and P. Tans, per.comm)

Figure 4: Locations of Stations Compared to Models.

Table 2. SF₆ mole fraction at measurement sites: observations and model simulations.

Station	Latitude	Longitude	Observations (pptv)	CCC (pptv)	CSU (pptv)	GFDL- GCTM (pptv)	GFDL-SKYHI (pptv)	GISS (pptv)	GISS-UViC (pptv)	MUTM (pptv)	NIRE (pptv)	TM2 (pptv)	TM3 (pptv)
Neumayer	-71.0	-8.0	2.79	2.84	2.79	2.82	2.83	2.81	2.77	2.82	2.82	2.78	2.79
Tierra del Fuego [‡]	-54.9	-68.5	2.64	2.84	2.79	2.82	2.83	2.82	2.78	2.83	2.83	2.78	2.80
Cape Grim, Tasmania	-40.7	144.7	2.80	2.86	2.80	2.84	2.85	2.83	2.80	2.84	2.85	2.80	2.83
Barbados [‡]	13.2	-59.4	2.93	3.02	2.95	3.06	3.02	2.98	3.07	2.98	3.10	3.06	3.04
Guam [‡]	13.4	144.8	2.96	2.99	2.92	3.03	2.99	2.97	3.06	2.97	3.05	3.02	3.04
Kumukahi, Hawaii [‡]	19.5	-154.8	3.31	3.06	2.97	3.09	3.03	3.01	3.12	3.00	3.12	3.08	3.10
Izana	28.0	-16.0	3.09	3.14	3.03	3.17	3.09	3.06	3.14	3.04	3.22	3.13	3.20
Bermuda [‡]	32.4	-64.7	3.23	3.12	3.07	3.16	3.12	3.09	3.20	3.04	3.24	3.12	3.19
North Carolina Tower ^{‡*}	35.4	-77.4	3.56	3.47	3.15	3.51	3.28	3.13	3.25	3.24	3.54	3.30	3.54
Tae Ahn Peninsula ^{‡*}	36.7	126.1	3.43	3.31	3.16	3.28	3.65	3.14	3.26	3.13	3.34	3.23	3.46
Azores [‡]	38.8	-27.1	2.99	3.00	3.01	3.01	3.02	3.03	3.04	3.04	3.05	3.06	3.06
Utah ^{‡*}	39.9	-113.7	3.22	3.18	3.05	3.35	3.19	3.10	3.19	3.07	3.24	3.15	3.23
Wisconsin Tower ^{‡*}	45.9	-90.3	3.38	3.32	3.10	3.28	3.27	3.15	3.34	3.18	3.39	3.21	3.63
Hungary ^{‡*}	47.0	16.4	3.16	3.56	3.17	3.79	3.39	3.21	3.41	3.26	3.70	3.29	3.99
Fraserdale ^{‡*}	50.0	-82.0	3.21	3.24	3.07	3.24	3.23	3.13	3.29	3.09	3.27	3.17	3.27
Mace Head, Ireland [‡]	53.3	-9.9	3.31	3.19	3.08	3.30	3.21	3.11	3.25	3.08	3.32	3.20	3.29
Cold Bay, Alaska [‡]	55.2	-162.7	3.20	3.15	3.04	3.18	3.15	3.08	3.18	3.07	3.18	3.14	3.21
Alert	82.5	-62.5	3.15	3.16	3.05	3.19	3.15	3.09	3.19	3.08	3.21	3.16	3.22
Atlantic transect 1	39.5	-14.3	3.24	3.20	3.10	3.40	3.13	3.13	3.26	3.11	3.42	3.25	3.35
Atlantic transect 2	29.2	-17.1	3.24	3.23	3.10	3.22	3.13	3.12	3.21	3.09	3.34	3.21	3.25
Atlantic transect 3	20.1	-21.2	3.22	3.19	3.08	3.18	3.10	3.11	3.18	3.07	3.28	3.18	3.22
Atlantic transect 4	9.4	-23.7	3.04	3.15	3.02	3.12	3.09	3.02	3.12	3.02	3.20	3.02	3.07
Atlantic transect 5	-0.2	-18.5	2.98	2.97	2.93	2.99	2.96	2.95	2.93	2.94	2.96	2.92	2.93
Atlantic transect 6	-11.7	-7.3	2.89	2.94	2.90	2.94	2.94	2.91	2.90	2.92	2.92	2.88	2.91
Atlantic transect 7	-18.8	8.0	2.93	2.92	2.90	2.96	2.93	2.93	2.91	2.92	2.91	2.88	2.91
Atlantic transect 8	-25.9	10.1	2.91	2.92	2.89	2.92	2.93	2.90	2.90	2.92	2.91	2.88	2.90
Atlantic transect 9	-32.7	8.6	2.91	2.92	2.88	2.92	2.92	2.90	2.87	2.91	2.90	2.87	2.89
Atlantic transect 10	-39.5	7.9	2.88	2.92	2.88	2.91	2.92	2.89	2.87	2.91	2.90	2.87	2.89
Atlantic transect 11	-48.1	9.1	2.88	2.91	2.87	2.90	2.91	2.89	2.87	2.90	2.90	2.87	2.88
Atlantic transect 12	-56.6	9.1	2.90	2.91	2.87	2.90	2.91	2.89	2.86	2.90	2.90	2.86	2.88

[‡] Value back-extrapolated to 1993 annual mean via OLS fit to available measured data.

^{*} Not considered a "marine boundary location".

Simulated Surface Mixing Ratio: Comparison to Observations

Simulated surface mole fractions display a pole-to-pole difference of about 10% (0.3 pptv) from the Arctic to the Antarctic (Figure 5). Most of the models are reasonably successful in capturing the observed magnitude of this meridional gradient, with considerably less model-to-model variance than was apparent in the zonal mean distributions presented in TransCom 1 [Law *et al.*, 1996]. This may be due to improvements in some of the models since the earlier experiment, and may also reflect that one model (CSIRO9) which produced much stronger than average meridional gradients at the surface was not included in TransCom 2. Less variation is expected for "clean air" sites in the marine boundary layer than the surface zonal means which were compared in TransCom 1. The elevated SF₆ values at Kumukahi and the Azores may be an artifact introduced by the extrapolation of data collected in 1996 back in time to compare to the 1993 simulations.

An additional observational constraint on the degree of tracer accumulation in the source regions is provided by the longitudinal gradient through the "plume" of elevated SF₆ concentrations extending eastward from the European source region across Eurasia (Figure 6). The models with the highest concentration maxima (NIRE, GFDL-GCTM, TM3, and possibly CCC) all overestimate the gradient between Moscow and central Siberia as measured by the railroad transect [Crutzen *et al.*, 1997]. This could be indicative of insufficient advective transport in the vicinity of strong horizontal concentration gradients. Alternatively, it could indicate excessive vertical trapping, as shown by the higher global mean surface mole fractions in these models as discussed above. Horizontal redistribution cannot account for these differences in the global mean surface mole fraction.

Meridional profiles of surface concentrations of anthropogenic tracers have frequently been interpreted in terms of meridional transport and interhemispheric exchange. Such an interpretation is complicated for the results presented here because both the simulations and the observations show considerable longitudinal variation. Interhemispheric gradients estimated from these data will depend strongly on the locations of observing stations, and may reflect the degree to which

tracer mass is retained in the source regions against zonal or vertical mixing as well as meridional mixing. We note that the area-weighted global surface mean mole fractions are significantly lower for those models with the weakest meridional gradients (CSU, MUTM, GISS) than for those with the strongest gradients (NIRE, GFDL-GCTM, TM3).

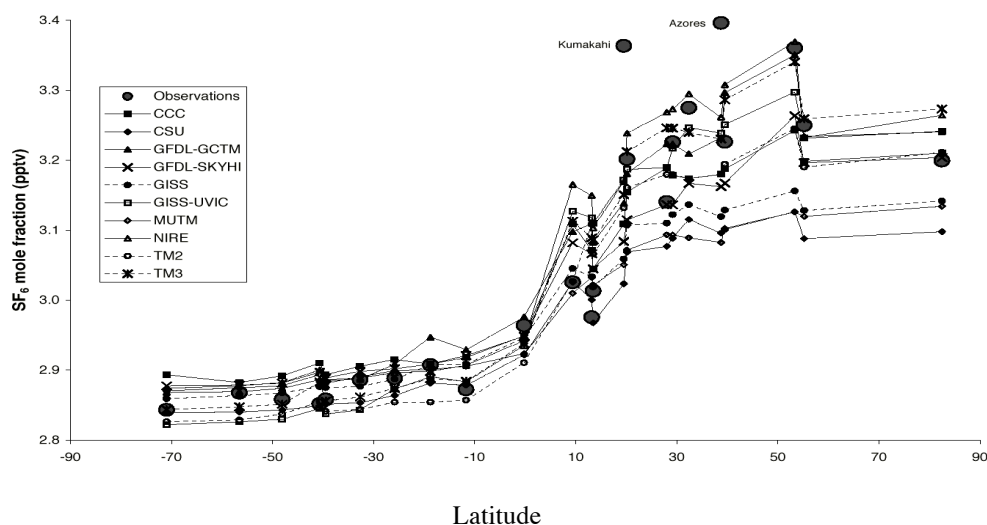


Figure 5: MBL Surface SF₆ Observations (time adjusted) and Model Predictions (emissions adjusted).

None of the models simultaneously satisfies the constraints of the meridional gradient in the marine boundary layer and the longitudinal gradient across Eurasia. This could be accomplished by more vigorous horizontal transport in the lower troposphere, reducing regional maxima in the regions, and increasing values in the remote MBL. The "less convective" models would have to compensate by allowing more vertical mixing of tracer to prevent overestimating the MBL data. Similarly, the "more convective" models would have to have reduced vertical mixing to prevent underestimates of the east-west gradient.

Zonal Mean Vertical and Meridional Structure

Zonal mean cross-sections of annual mean simulated mole fraction for each model are compared in Figure 7. All models show elevated mole fractions at the surface in the northern hemisphere source region. The models can be classified into two populations based on these cross-sections: one group (CSU, GISS, MUTM, and TM2) simulates relatively weak vertical gradients over the northern extratropics, whereas a second group (CCC, both GFDL models, GISS-UVic, TM3, and especially NIRE) simulate stronger vertical gradients over the source region. This probably reflects differences in the subgrid-scale parameterized transport by convection and diffusion.

The division of the models into a "strongly mixed" and a "weakly mixed" population also seems to explain many of the differences in simulated surface tracer distributions discussed above. The weakly mixed models tend to accumulate more SF₆ in the lower troposphere of the northern hemisphere, and thus have stronger surface meridional gradients than the strongly mixed models. The most strongly vertically mixed models (CSU, GISS, MUTM) tend to underestimate the surface mole fraction at most observing stations (cf. Figure 5). The more weakly mixed models (NIRE, TM3, and the GFDL models) are generally quite successful at simulating the observed meridional gradient in the remote marine boundary layer (Figure 5), but systematically overestimate SF₆ at continental sites and near the western end of the Siberian transect (Figure 6). These results suggest that differences in parameterized vertical transport among the models, rather than differences in resolved advection, may account for most of the differences in meridional structure at the surface.

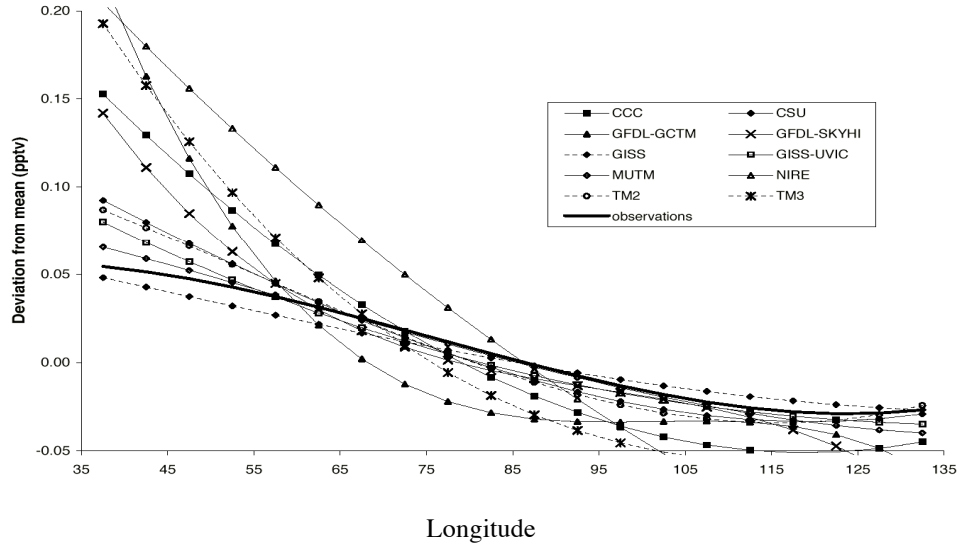


Figure 6: Siberian Rail Observations vs. Model Prediction (cubic fit)

It is difficult to decide which of these scenarios is closest to reality, because nearly all the observational data is at the surface and the most striking differences between the two populations of models is in their simulated vertical structure. Vertical profiles through the depth of the troposphere over the source regions would be extremely helpful in falsifying one of the populations of models. To date, the only published vertical profiles of SF₆ have been from stratospheric sampling programs [Harnisch *et al.*, 1996; Patra *et al.*, 1997], but these results provide almost no constraint on the behavior of the TransCom models with their tropospheric focus. A recent effort to measure vertical profiles in the troposphere over Tasmania (Ray Langenfelds, personal communication) may prove much more helpful in this regard, although a similar campaign over the northern hemisphere source region would provide a much stronger constraint.

All models show a reversed vertical gradient in the southern hemisphere, with SF₆ increasing with height. This suggests that southward penetration of SF₆ across the equator occurs primarily in the upper troposphere. Interestingly, this interhemispheric penetration is most pronounced for the less convective models that exhibit the strongest vertical gradient. This feature may reflect the fact that mean meridional overturning in the tropics associated with the Hadley cell can only achieve interhemispheric mixing to the degree that the upper and lower branches transport air with different SF₆ content. Rapid vertical mixing in the tropics would therefore be an effective *barrier* to interhemispheric transport, even in the presence of vigorous mass circulation. This interpretation is consistent with the experience of Heimann and Keeling [1989], who found that reducing convective transport of their tracers by 50% increased the interhemispheric transport of CO₂ in an earlier version of the TM series of models.

Interhemispheric Transport Mechanisms

To first order, the global distribution of a trace gas emitted primarily in the northern hemisphere by anthropogenic activity can be expressed in terms of a two-box mixing model. In this simplification, each hemisphere is represented as a well-mixed box and the mixing between them is represented in terms of an interhemispheric exchange time t_{ex} (e.g., [Czelpak and Junge, 1974; Heimann *et al.*, 1986; Weiss *et al.*, 1983]. Although this representation has been used to estimate atmospheric mixing from observed meridional profiles of trace gases, the value of t_{ex} is sensitive to the method of calculation [Jacob *et al.*, 1987; Law *et al.*, 1996; Weiss *et al.*, 1983] and to the meridional distribution of emissions of the tracer used [Plumb and McConalogue, 1988]. Despite these ambiguities, the interhemispheric exchange time remains a useful conceptual tool because it collapses all the transport mechanisms into a single parameter which can be compared across simulations and to observations.

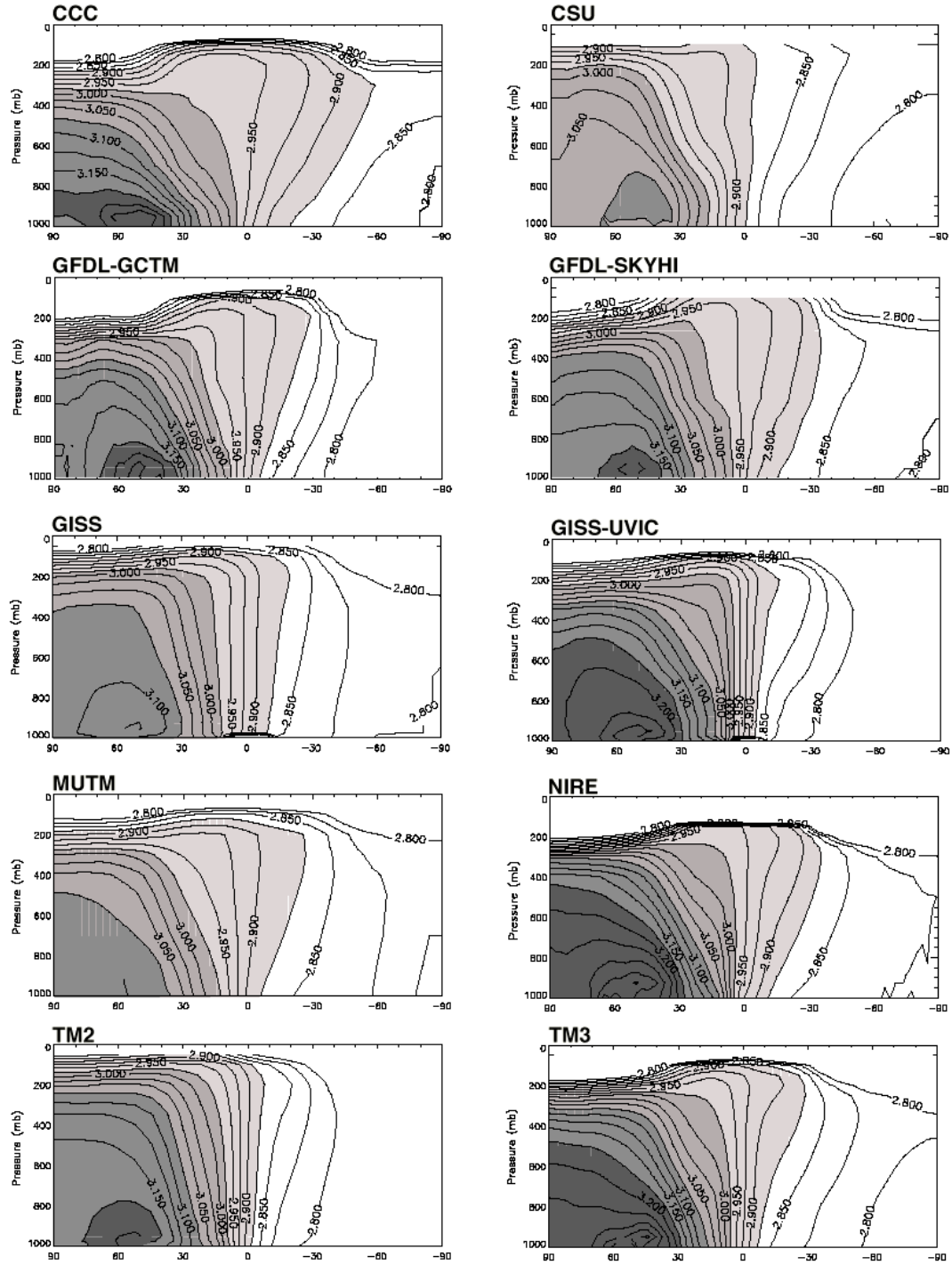


Figure 7: Annual and Zonal Mean SF₆ Mole Fraction (pptv)

Critical to the assessment of interhemispheric exchange time is the way in which the hemispheric mixing ratios are computed. Table 3 shows t_{ex} based on both model results and measurements comprising different definitions of the hemispheric mean SF₆ mixing ratios. Interhemispheric exchange times were calculated both for the October-November period, to facilitate comparison with the observational t_{ex} from the Atlantic transect, and as annual means, which are more

representative of overall model performance. To highlight relative differences among the models, the annual mean t_{ex} values are also indicated in terms of their "rank," with fastest interhemispheric transport indicated by 1 and the slowest by 10.

Table 3. Interhemispheric Transport Comparison

in years

October/November

Annual

	October/November					Annual				
	S-S t_{ex} (1-D)	t_{ex} (1-D)	t_{ex} (2-D)	t_{ex} (3-D)	t_{ex} (1-D)	Rank	t_{ex} (2-D)	Rank	t_{ex} (3-D)	Rank
CCC	1.31	1.88	1.53	0.57	1.14	5	1.53	5	0.58	2
CSU	0.90	0.91	1.01	0.66	0.90	2	1.18	2	0.72	4
GFDL-GCTM	1.46	2.06	1.51	0.71	1.32	6	1.66	6	0.83	6
GFDL-SKYHI	0.92	0.91	1.21	0.69	1.05	4	1.44	4	0.73	5
GISS	0.90	0.96	1.15	0.84	1.00	3	1.22	3	0.88	8
GISS-UVIC	1.47	1.76	1.97	1.40	1.60	8	1.95	8	1.28	10
MUTM	0.76	0.82	1.03	0.57	0.82	1	1.12	1	0.63	3
NIRE	1.98	3.93	2.46	1.06	1.72	10	1.95	9	0.84	7
TM2	1.42	2.08	2.24	0.56	1.33	7	1.75	7	0.50	1
TM3	1.60	1.93	2.01	1.20	1.54	9	1.99	10	1.04	9
Observations	1.34									

In the first case, labeled "S-S t_{ex} (1-D)", the hemispheric mean SF₆ mixing ratios were computed based on October/November 1993 Atlantic transect SF₆ measurements. All the measurement locations north (south) of the equator were averaged (weighted by the cosine of latitude) to achieve the northern (southern) hemisphere mean SF₆ mixing ratios. The monthly mean 1993 model predictions for the Atlantic measurement locations were retrieved and interpolation between the October mean and the November mean were made to achieve a value consistent with the transect measurement dates. As can be seen in the table, this leads to interhemispheric exchange times of roughly one to two years for both the steady-state case and the instantaneous case (labeled " t_{ex} (1-D)"). Note that this is the method used to estimate interhemispheric exchange from field programs, and that it implicitly assumes that each point measurement is both zonally and vertically representative. Figure 7 clearly demonstrates that this is not the case for SF₆ in the models. The assumption that vertical and longitudinal variations can be neglected in the calculation of a two-box mixing time is probably quite unrealistic in nature as well.

The average hemispheric SF₆ mole fractions were also computed as surface-area weighted means (for the models only), and used to calculate an exchange time labeled " t_{ex} (2-D)" in the table. The interhemispheric exchange time calculated from all surface locations is larger than the one-dimensional case for all the models. This reflects the higher mole fractions in longitudinal regions strongly influenced by SF₆ source areas such as the eastern portion of North America and Western Europe. The interhemispheric exchange time calculated in this way implicitly assumes that each surface point represents a column mean. Note that the ranking of the t_{ex} values among models changes very little in going from station-based 1-D estimation to the full 2-D surface global mean mole fractions. The only change in the relative strengths of apparent

interhemispheric exchange from the 1-D to 2-D cases is that NIRE and TM3 have switched positions for the slowest among the suite of models.

The extent to which t_{ex} increases over the one-dimensional case also reflects the magnitude with which the models mix SF₆ zonally and vertically. For example, those models that exhibit strong vertical mixing exhibit two-dimensional t_{ex} times that are less affected by the inclusion of source regions in the northern hemisphere mean SF₆ mole fraction, because they retain less tracer near the surface in the source regions. Hence, their two-dimensional t_{ex} times do not increase as much over the one-dimensional case as is the case for those models with less vigorous vertical mixing. The relative change in t_{ex} for the GISS and GFDL-SKYHI models suggest this dynamic, for example. Both models have a nearly identical one-dimensional t_{ex} time yet the two-dimensional values diverge with the more vertically-mixed model, GISS, increasing to a t_{ex} of 1.22 years versus the larger GFDL-SKYHI value of 1.44 years.

Finally, t_{ex} was estimated by incorporating three-dimensional, mass-weighted mean mixing ratios for the northern and southern hemispheric mean SF₆ values. Interhemispheric exchange times derived in this way are true to the spirit of the two-box mixing model in that they represent the true hemispheric mean concentrations in each box, but still violate the well-mixed assumption. Not surprisingly, the interhemispheric exchange times calculated from 3D means are much lower than their 2D analogs, reflecting both the lesser absolute mixing ratio in the northern hemisphere and the diminished interhemispheric gradient of SF₆ aloft in all the models.

Using the full three-dimensional hemispheric means to calculate the two-box exchange time produces shifts in the relative intensity of inferred interhemispheric exchange among the models. These changes are much more significant than the changes in the relative ranks among models in going from a 1-D calculation to a 2-D calculation. Models that exhibit generally greater vertical mixing tend to have the lowest t_{ex} values (CSU, MUTM, and GISS), but some models behave very differently in 3D than we inferred from 2D means. The CCC model has one of the slowest exchange times as estimated from surface gradients, yet is one of the fastest when true mass-weighted means are used. The GISS-UVic model, on the other hand, exhibits the slowest t_{ex} in 3D, though has only the fourth-fastest t_{ex} in 2D. NIRE has by far the slowest t_{ex} when surface means are used, yet is faster than either GISS-UVic or TM3 when the full mass-weighted hemispheric mean values are used.

The exchange time estimated from surface values, especially at only a small number of longitudes, is a clearly poor predictor of true interhemispheric mixing in these models. The fact that the relative intensity of interhemispheric mixing is nearly unchanged from the 1-D to the 2-D case, but changes dramatically from the 2-D case to the 3-D case indicates that differences in vertical structure among the models dominate the differences in true interhemispheric exchange.

Interhemispheric exchange time was also estimated for many of the same models from the fossil fuel experiment in TransCom 1 [Law *et al.*, 1996]. In general, most models that participated in both experiments showed slower exchange times for SF₆ than for fossil fuel CO₂. This must be interpreted with care however, because (1) several of the models have been modified significantly between the two experiments, and (2) Law *et al.* [1996], used a steady-state approach to calculate the exchange times. Nevertheless, our results confirm the general TransCom 1 results of Law *et al.*, [1996]: t_{ex} increases from station-based 1-D estimates to a full 2-D surface mean, but using the full 3-D mass-weighted mean mixing ratios produces the fastest exchange time estimates. The increase from estimates based on data collected in the remote MBL to the 2-D estimate reflects the inclusion of regional concentration maxima in source regions, and the decrease from 2-D to 3-D estimates removes the confounding effects of vertical tracer gradient that can so easily be misinterpreted as meridional gradients.

Another approach to the diagnosis of interhemispheric transport is to decompose the total meridional tracer transport into contributions by the time-averaged zonal *mean motion* (e.g., by the Hadley and Ferrel Cells); the *standing eddies* (time-averaged deviations from the zonal mean that span a range of longitudes, such as blocking highs, the Aleutian low, and the Asian Monsoon); and the *transient eddies* (deviations in both space and time from the mean flow, such as those caused by winter storms in the middle latitudes). We performed this decomposition for a subset of the SF₆ simulations (Figure 8).

The total column integrated resolved meridional transport is not very different among the models, and is in fact constrained to balance the integrated surface emissions. The only major exception to this statement is the GISS model, which accomplishes much of its meridional transport via parameterized subgrid-scale horizontal diffusion. In all cases, meridional

transport by the mean motion, standing eddies, and transient eddies are all significant, though the dominant mechanisms vary considerably across models and by season.

Vertically and Zonally Integrated Meridional Transport

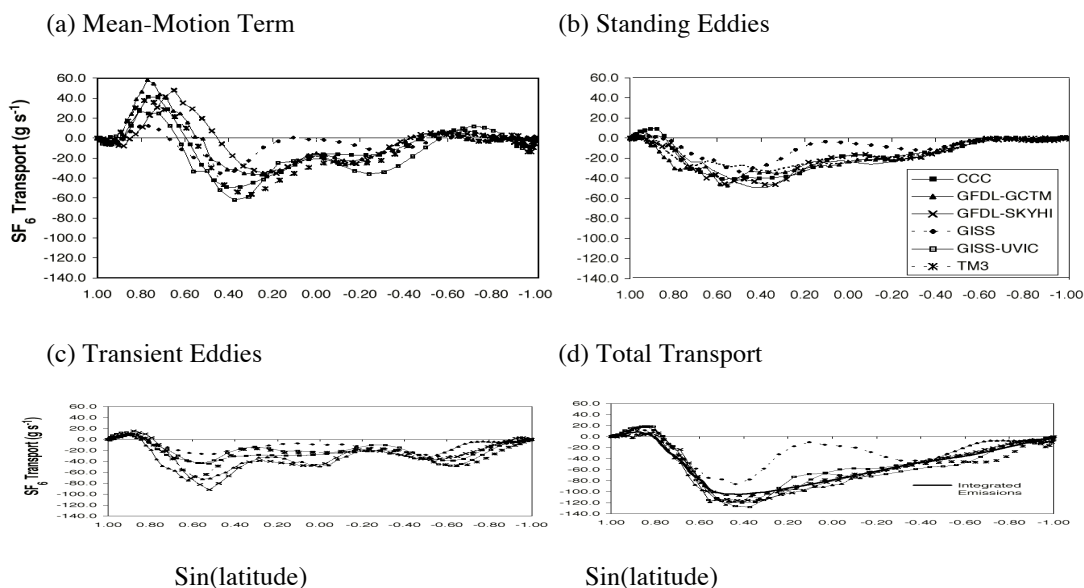


Figure 8

Conclusions from Phase 2:

In contrast to the results of TransCom 1, there was less spread in the simulated north-south tracer gradient in the remote marine PBL ($\sim 50\%$ vs. $\sim 100\%$ for the fossil fuel experiment in TransCom 1). Some of this "convergence" reflects model development, and some reflects a different suite of models. Most of the models are reasonably successful in reproducing the "background" observations of SF₆. Exceptions are the models which exhibit excessive vertical tracer transport by parameterized convection; these underestimate marine boundary layer values. Many of the models are less successful in continental locations near sources, where most models significantly overestimate SF₆. The more convective models match the observations better at these continental sites than do the less convective ones, but these results should be interpreted with caution because the details of the local-scale emissions field are not captured by the population-based distribution used here.

Our results generally agree with the TransCom 1 findings that strong meridional gradients in simulated fossil fuel CO₂ at the surface were systematically associated with weak meridional gradients in the upper troposphere, and vice versa. In addition, the importance of vertical transport for interpreting observed meridional structure at the surface was underlined by the TransCom 1 biosphere experiment, which showed that models with a large degree of vertical trapping of fossil fuel CO₂ exhibited stronger than observed meridional gradients in the amplitude of biospheric CO₂.

Although there are distinct differences in the intensity of interhemispheric exchange among the models, these differences cannot be understood in terms of spatial distributions of tracer at the surface. The ranking of estimated t_{ex} using 1-D station data or the 2-D surface global mean mole fraction is nearly the same, whereas the true t_{ex} calculated from 3-D mass-weighted mean mole fractions produces an entirely different ranking. This result confirms that differences in interhemispheric exchange times among the models are dominated by differences in vertical structure. Observed meridional gradients of tracers should be interpreted with caution, since a two-box mixing model derived from surface observations can clearly produce qualitatively false results in which vertical mixing is misconstrued as interhemispheric transport.

Modelling the Methane Cycle

Insights provided by the results of the Transport Code Intercomparisons will set the stage for developing models of the methane cycle. Methane has been identified as a major climate gas in the atmosphere and a key compound in the chemical processes affecting tropospheric ozone chemistry. The recent IPCC assessment (1994) has strongly upgraded its climatic role compared to previous assessments, mainly due to its chemical impact on the atmosphere. Measurements have clearly demonstrated that its atmospheric concentration has been increasing over the last century, and is now believed to be more than a factor of two higher than the pre-industrial values. This increase has undoubtedly had a profound impact both on climate and atmospheric chemistry. Methane has increased over the last decade by 0.8% per year on average, while the rate over the last few years has been substantially less. The cause of the long term trend, and the decrease in recent years are not fully understood. Both could be either the result of changes in the magnitude of surface sources or in the atmospheric sinks. Anthropogenic sources of methane are related to agricultural and industrial activities. In particular, there is poor quantification of the potential changes in soil emissions and consumption associated with changes in land-use and other modifications in terrestrial ecosystems.

Methane is simpler in one respect than the CO₂ cycle in that it does not have large and poorly constrained sinks in the ocean and terrestrial systems. However, methane is not conservative in the atmosphere, being subject to oxidation. The atmospheric chemical interaction of methane is being studied in a joint GAIM/IGAC 3-D model intercomparison activity. This study focuses on the atmospheric response to changes in emissions, and therefore links naturally to the proposed methane cycle study. For instance, 3-D model estimates of temporal and spatial variations of methane oxidation can be used together with observed variations of methane to estimate emissions from wetlands.

As a first step in exploring the methane cycle, we have focused on terrestrial sources, the largest of which are natural and artificial wetlands. The methane budget is strongly affected by wetland sources, both natural and anthropogenic. Consequently, in order to correctly account for methane terms in global biogeochemical models, it is essential to understand the role of wetlands in methane production as well as the effect of changing wetland distribution. The extent of wetlands is uncertain because there is no clear basis for identification and functional classification of wetlands on a global scale. In addition, the areal extent of wetlands is being modified as a result of land-use changes, so that once a globally consistent classification scheme is established, the areal distribution must be monitored and recompiled. New data are becoming available from remote sensing which provide a global perspective on wetland distribution and classification, but which are not yet reconciled with ground-based ecological and hydrological data. There remains a gulf between the scale of trace gas emissions as measured from the ground, and the measurable atmospheric effects of this based on remote sensing. These conceptual and technical discontinuities need to be reconciled.

As a first step, we have constructed a wetland functional classification scheme [*IGBP report 46*]. This, in conjunction with developments in understanding of emissions from rice paddies and ruminants will provide the input boundary flux for atmospheric methane necessary for climate and biogeochemical models. This flux will be balanced against oxidation and atmospheric accumulation, as modulated by atmospheric transport, to be provided by the transport codes as tested in Phase 1.

With sources, sinks, and atmospheric transport terms in hand, methane cycle models can be subsequently developed which will accurately predict atmospheric methane concentration evolution in response to human activity as well as natural causes.

General Conclusions

We have made significant progress in understanding the mechanisms for differences among the models. Our results underline the importance of subgrid-scale parameterized vertical transport, even for the interhemispheric transport of a long-lived passive tracer. Differences in the meridional gradient of SF₆ at observing sites in the remote marine BL among models cannot be explained in terms of differences in meridional transport or interhemispheric mixing. Rather, a combination of vertical and meridional transport is involved, with meridional gradients at the surface associated with strong vertical gradients in the source regions. The differences among models are best explained in terms of differences in the intensity of subgrid-scale parameterized vertical transport rather than in terms of distinctions between CTMs and GCMs, or the use of analyzed wind observations rather than GCM simulated winds for the resolved transport.

The vertical distribution of atmospheric trace gases is much more difficult and expensive to quantify through observing programs than is the horizontal spatial structure at the surface. Observational data collected at the surface may easily be misinterpreted in terms of meridional transport and interhemispheric mixing unless a better constraint is placed on vertical profiles in areas of elevated surface concentrations and on meridional gradients aloft. A series of regular vertical profiles of SF₆ over western Europe and the northeastern United States would provide a useful constraint for model validation. If such a program were combined with periodic meridional profiles in the middle to upper troposphere, it would be feasible to falsify one or the other of the two "families" of simulations presented here.

We note that both TransCom 1 and TransCom 2 have found significant differences in simulated meridional and especially vertical tracer structure that result entirely from differences in the simulated transport among models. Some of the models in these experiments are also being used to simulate the distribution of reactive trace gases in the troposphere, and interpretation of the results of such experiments must be done with caution since transport differences are involved with differences in reactive chemistry in such experiments. A systematic program to quantify the 3-dimensional distribution of an easy-to-measure nonreactive tracer such as SF₆ would be prudent to allow the simulated transport to be calibrated among these models. Such a program would add significant value to observing programs which measure reactive gases.

One important aspect of the transport model incorporation was the striking difference between models in the simulated surface meridional gradient of CO₂ in the TransCom 1 biospheric experiment. The Arctic-to-Antarctic CO₂ gradient in that experiment varied from 2.5 ppm in models with strong rectification (CSU, CCM2, NIRE) to less than 0.5 ppm for those models with weak rectification (GISS, MUTM, TM2), to -1.5 ppm for the ANU model, which appears to exhibit negative rectification [Law *et al.*, 1996]. This important difference has a direct and significant bearing on the use of these models in CO₂ inversion studies [Denning *et al.*, 1996; Denning *et al.*, 1995]. Unfortunately, neither the SF₆ experiment nor a ²²²Rn calibration can directly address the question of rectification. Correct vertical transport by subgrid-scale processes is a necessary condition for correct simulation of rectification, and can be tested with better data on the vertical and seasonal changes in tropospheric ²²²Rn. Terrestrial CO₂ flux is different from ²²²Rn in that it changes sign from night to day and from summer to autumn; it is the *covariance* between flux and the vertical transport that must be simulated correctly. Calibrating this aspect of model transport may best be accomplished at smaller scales using intensive field data rather than global simulations using occasional and widely scattered column constraints.

The use of tracer transport codes for atmospheric inversion studies is a valuable tool that can add significant information about sources and sinks of atmospheric trace gases. Such calculations currently face considerable uncertainty due to differences in simulated transport. A worthwhile future goal would be to quantify the uncertainty in carbon cycle inversion calculation arising from the transport directly, through an inversion intercomparison.

Appendix: Model Descriptions

CCC

The simulations submitted by the Canadian Climate Centre were performed with CCC GCMII [McFarlane *et al.*, 1992], which is a spectral model with T32 triangular truncation and 10 hybrid sigma/pressure vertical levels with an upper boundary at 10mb. The tracer advection was performed spectrally without any hole filling. The very accurate transports of the spectral method (as for example measured by the local closure of the column budget), are found to outweigh occasional Gibbs overshoots, which are not an impediment for a purely passive tracer such as SF₆, as long as one keeps in mind that one is dealing with a truncated spectral representation. Parameterized vertical transport consists of stability-dependent vertical diffusion and a simple moist convective adjustment scheme, both of which are consistent with what is done for moisture. A small amount of horizontal diffusion is applied spectrally to high wave numbers only and helps to control the spatial spectrum of the tracer. The horizontal diffusivity of tracers is taken to be the same as that for moisture in the absence of any other information.

CSU

The Colorado State University (CSU) General Circulation Model (GCM) was derived from the UCLA GCM by D. Randall and colleagues. The model includes parameterizations of the effects of moist cumulus convection [Randall and Pan, 1993] and cloud microphysics [Fowler *et al.*, 1996]. A key feature of the model is its formulation in a modified sigma coordinate which is defined such that the top of the PBL is a coordinate surface [Suarez *et al.*, 1983]. The depth of the turbulent PBL is determined as a prognostic variable in the model using a second-order bulk method based on the turbulence kinetic energy equation [Randall *et al.*, 1992]. Surface fluxes of momentum, energy, water, and carbon at land grid points are calculated on-line using the Simple Biosphere Model SiB2, [Randall *et al.*, 1996; Sellers *et al.*, 1996].

Tracer transport includes large-scale advection and sub-grid scale vertical transport by penetrative cumulus convection, dry convective mixing, and boundary-layer turbulence and entrainment [Denning *et al.*, 1996]. Cumulus convection now originates in multiple model layers, and transports tracers in a penetrative manner to any higher layer in the troposphere. Tracer advection is calculated by a second-order, centered-in-space, leapfrog-in-time scheme. At the PBL top, a first-order upstream scheme is applied separately for turbulent entrainment and loss of tracer mass from the PBL due to cumulus mass flux. After each 10 leapfrog timesteps, we perform a Matsuno step to suppress the computational mode. TransCom SF₆ experiments were integrated on a 4° x 5° grid with 17 levels, at a time step of 5 minutes.

GFDL-GCTM

The GCTM is driven by 6-hour time-averaged winds and a consistent total column precipitation field that was generated by a parent general circulation model (GCM) integrated for one year without diurnal insolation. Therefore, the GCTM can not realistically simulate atmospheric fluctuations with periods shorter than six hours or examine interannual variability. Both the parent GCM and the GCTM have the same resolution, a horizontal grid size of ~265 km, and 11 vertical levels at standard pressures of 990, 940, 835, 685, 500, 315, 190, 110, 65, 38, and 10 mb. The GCTM includes parameterizations designed to incorporate the effects of horizontal sub-grid scale transport, as well as vertical mixing by dry and moist convection throughout the troposphere and a vertical wind-shear dependent turbulent transport in the boundary layer (for details see Appendix A of Levy *et al.*, [1982], and Section 2 of Kasibhatla *et al.*, [1993].

GFDL-SKYHI

The GFDL SKYHI model has a long history of development, and has a variety of options for grid size and advection scheme [Mahlman and Strahan, 1994; Mahlman and Umscheid, 1984]. Climatology of the SKYHI model is described in detail in [Hamilton *et al.*, 1995].

The present standard version has 40 vertical layers, with the lowest thirteen layers centered at 0.08, 0.27, 0.74, 1.4, 2.2, 3.1, 4.1, 5.2, 6.5, 7.8, 9.1, 10.5, and 12.0 km altitude over the sea, and with the lowest 10 levels following surface topography. It has a horizontal grid size of 3° latitude by 3.6° longitude. The model uses specified values of sea surface temperature but calculates land temperature prognostically. The model calculates the moisture content prognostically as well.

The SKYHI model calculates radiative transfer and the absorption and emission of radiation by O₃, H₂O and CO₂ molecules, and clouds. The radiation was calculated for time interval of 4 hours in the SF₆ experiment. Ozone and cloud distribution and ice-free surface albedo are prescribed.

Surface exchanges of heat, moisture, and momentum are parameterized, based on the Monin-Obhukov similarity theory, with bulk aerodynamic formulas. Sea surface roughness is calculated from wind stress while land roughness is a constant specified value. Parameterization of subgrid-scale transports uses horizontal diffusivity that is proportional to the magnitude of the horizontal velocity deformation, and uses vertical diffusivity that is proportional to the magnitude of the vertical wind shear and is a function of the moist bulk Richardson number. In a recent modification of the SKYHI model, maximum vertical diffusivity is calculated for chemical tracers that is allowed by the centered differencing scheme without numerical instability, and is used to represent the rapid vertical mixing of SF₆ under unstable conditions (J. Mahlman, personal communication).

GISS

The GISS tracer model was developed in the late 1970's and early 1980's, and its design reflected the computational capabilities of that era. The circulation commonly used is derived from the 1984 version of the GISS GCM [Hansen *et al.*, 1983], run at a resolution of 4° degrees latitude x 5° degrees longitude with 9 sigma levels in the vertical. The horizontal mass fluxes from the GCM were accumulated over 4 hour periods and archived. Advection is by the linear upstream scheme of [Russell and Lerner, 1981]. From the GCM, the total number of mixing events in a month between two vertical layers is recorded for moist and dry convection. The monthly convective frequency is then translated into a fraction of the gridbox air mass that mixes every time step (4 hours). The approach was necessitated by computer memory limitations and was adopted to reproduce on-line GCM simulations of tracer concentrations at monthly means, but not at higher frequencies. To match the interhemispheric transport time for CFC's, [Prather *et al.*, 1987] introduced a sub-grid scale horizontal diffusion based on the depth of moist convection. The version of the GISS tracer model used for TransCom 1 employs the same GCM circulation statistics at 4°x 5° resolution, but the mass fluxes were aggregated to 8°x10°. In this study, the tracer model was run at the GCM resolution of 4°x 5°.

GISS-UVic

The GISS-UVic tracer model is derived from the 1996 version of the GISS GCM [Hansen, 1997]. The resolution of the GCM and the tracer model is 4°x 5° with 9 sigma levels in the vertical. The 1996 version of the GCM has many improved treatments of atmospheric physics compared to the 1984 version. Important for tracers is the parameterization of moist convection [Yaolin and Yuanqing, 1993], clouds [DelGenio *et al.*, 1996], and the planetary boundary layer [Hartke and Rind, 1997]. Moist convection [Yaolin and Yuanqing, 1993] is linked to mass flux closure as well as stability of the column; convective downdrafts, and mesoscale cirrus anvils are included. From the GCM, large scale fields of horizontal mass fluxes are archived every hour for calculation of large scale advection in the tracer model. The linear upstream scheme of Russell and Lerner [1981] is used. At every GCM physics time step (1 hour for moist and dry convection), the tracer model duplicates exactly the GCM calculation of mixing by moist convection and dry convection. For moist convection, this is achieved by archiving the 3D fields of temperature and humidity just before the hourly call to moist convection in the GCM, and repeating the GCM moist convection subroutine in the tracer code, which then mixes, entrains and detrains tracers in addition to temperature and humidity according to the conditions captured in the temperature and humidity profiles. For dry convection, the height of planetary boundary layer is archived every hour. No explicit horizontal or vertical diffusion is included.

MUTM

The Melbourne University Tracer Model (MUTM), described by Law *et al.* [1992], is an offline transport model derived from the Melbourne University General Circulation Model (GCM). It is a spectral model with rhomboidal 21 wave resolution and 9 levels. The transport is forced by daily winds from a control run of the Melbourne University GCM. There is no diurnal cycle but tests using CO₂ have shown that transport is similar for 6 hourly winds with a diurnal cycle. Vertical diffusion is parameterized using the same mixing length scheme as used in the GCM for moisture. Convective transport is parameterized based on daily convection statistics from the GCM.

NIRE

NIRE-CTM-96 is a modified version of NIRE-CTM-93 [Taguchi, 1996]. Major modifications are vertical coordinates from sigma to pressure-sigma mixture and explicit use of tropopause diagnosed from ECMWF temperature profiles. Turnover time of stratosphere in NIRE-CTM-96 is 1.5 years which is significantly longer than 0.5 years of NIRE-CTM-93.

TM2

The Tracer Model version 2 is modified from TM1, which was adapted by Heimann and Keeling [1989] from the GISS model, for use with analyzed winds. TM2 is an offline CTM which differs from TM1 in its subgrid-scale parameterized vertical transport. TM2 simulates vertical transport by stability-dependent vertical diffusion following Louis [1979], and by cumulus convection following Tiedke [1989]. Advection by the mean flow is calculated using the slopes scheme [Russell and Lerner, 1981]. The experiments described in the present paper were performed on a horizontal grid of $7.5^\circ \times 7.5^\circ$ (latitude-longitude), with 9 levels in the vertical, and a time step of 3 hours. Resolved transport was forced with winds specified from ECMWF analyses for 1993, which were updated every 12 hours.

TM3

The Tracer Model version 3 is the successor of the atmospheric transport model TM2 [Heimann, 1995]. It computes in an off-line mode the transport of a tracer based on the fields from three-dimensional meteorological analyzes or from the output of an atmospheric general circulation model. The version used in the TransCom 2 experiments has a horizontal resolution of 5° longitude by 3.8° latitude and a hybrid (sigma-pressure) vertical coordinate with 19 layers from the surface to the top of the atmosphere (100mb). The meteorology used in the SF₆ simulations is from a T42 control run of the ECHAM3 climate model, stored at a temporal resolution of 6 hours. Resolved transport is computed numerically with the slopes scheme [Russell and Lerner, 1981]. Subgrid scale transport in the vertical is computed by stability dependent vertical diffusion [Louis, 1979] and cloud convection [Tiedke, 1989] Both schemes are identical to the schemes employed in the "parent" climate GCM. There is no horizontal diffusion. Diurnal cycles are only marginally resolved in the present version due to the coarse temporal resolution of the input fields.

References:

- Ciais, P., P. Tans, J. White, M. Trolier, D. Schimel, and others, Partitioning of Ocean and Land Uptake of CO₂ as Inferred by Delta-C-13 Measurements from the NOAA Climate Monitoring and Diagnostics Laboratory Global Air Sampling Network, *J. Geophys. Res.*, *100*, 5051-5070, 1995.
- Conway, T.J., P. Tans, L. Waterman, K. Thoning, D. Buanerkitzis, K. Masarie, and N. Zhang, Evidence for interannual variability of the carbon cycle from the NOAA/CMDL global air sampling network, *J. Geophys. Res.*, *99D*, 22831-22855, 1994.
- Crutzen, P., T. Rockmann, C. Brenninkmeijer, and P. Neeb, Ozonolysis of nonmethane hydrocarbons as a source of the observed mass independent oxygen isotope enrichment on tropospheric CO₂, *J. Geophys. Res.-Atmosph.*, *103*, 1463-1470, 1998.
- Crutzen, P.J., N.F. Elansky, M. Hahn, M. Golitsyn, and e. al, Trace gas measurements between Moscow and Vladivostok using the Trans-Siberian Railroad, *Atmos. Chem.*, *in press*, 1997.
- Czelpak, G., and C. Junge, Studies of interhemispheric exchange in the troposphere by a diffusion model., *Adv. Geophys.*, *18B*, 57-72, 1974.
- DelGenio, A.D., V. Alekseev, V. Dymnikov, V. Galin, and E.M. Volodin, Cloud feedback in atmospheric general circulation models- an update, *J. of Geophys. Res.-Atmos.*, *101*, 12791-12794, 1996.
- Denning, A.S., G.J. Collatz, C.G. Zhang, D.A. Randall, and e. al, Simulations of Terrestrial Carbon Metabolism and Atmospheric in a General Circulation Model. 1. Surface Carbon Fluxes, *Tellus Series B-Chemical and Physical Meteorology*, *48*, 521-542, 1996.
- Denning, S., I. Fung, and Randall, Latitudinal gradient of atmospheric CO₂ due to seasonal exchange with land biota, *GISS Research Publications*, 49-50, 1995.
- Denning, S., and D. Randall, Investigations of transport, sources, and sinks of atmospheric CO₂ using a general circulation model, Department of Atmospheric Science, Colorado State University, Fort Collins, CO., 1995.
- Enting, I., and J. Mansbridge, Seasonal sources and sinks of atmospheric CO₂. Direct inversion of filtered data, *Tellus*, *39B*, 318-325, 1989.
- Enting, I., and J. Mansbridge, Latitudinal distribution of sources and sinks of CO₂: Results of an inversion study, *Tellus*, *43B*, 156-170, 1991.
- Enting, I., C. Trudinger, and R. Francey, A synthesis inversion of the concentration and delta 13C of atmospheric CO₂, *Tellus*, *47B*, 35-52, 1995.
- Fowler, A.C., V. Alekseev, V. Dymnikov, V. Galin, and E.M. Volodin, Cloud feedback in atmospheric general circulation models-an update, *J. of Geophys. Res.-Atmos.*, *101*, 12791-12794, 1996.
- Francey, R.J., P. Tans, C. Allison, I. Enting, J. White, and M. Trolier, Changes in oceanic and terrestrial carbon uptake since 1982, *Nature*, *373*, 326-330, 1995.
- Fung, I., J. John, J. Lerner, E. Matthews, and e. al., 3-Dimensional model synthesis of the global methane cycle, *J. Geophys. Res.*, *96*, 13033-13065, 1991.
- Fung, I., K. Prentice, E. Mathews, J. Lerner, and G. Russell, Three-dimensional tracer model study of atmospheric CO₂: Response to seasonal exchanges with the terrestrial biosphere., *J. Geophys. Res.*, *88*, 1281-1294, 1983.
- Fung, I., C. Tucker, and K. Prentice, Application of very high resolution radiometer vegetation index to study atmosphere biosphere exchange of CO₂., *Journal of Geophysical Research*, *92*, 2999-3015, 1987.
- Geller, L.S., J.W. Elkins, J.M. Lobert, A.D. Hurst, and e. al, Tropospheric SF₆: Observed latitudinal distribution and trends, derived emissions and interhemispheric exchange time, *Geophys. Res. Lett.*, *24*, 675-678, 1997.
- Hamilton, K., R.J. Wilson, J.D. Mahlman, and L.J. Umscheid, Climatology of the SKYHI troposphere- stratosphere-mesosphere general circulation model, *Journal of the Atmospheric Sciences*, *52*, 5-43, 1995.
- Hansen, Forcings and chaos in interannual to decadal climate change, *Journal of Geophysical Research*, *in press*, 1997.
- Hansen, J., G. Russell, D. Rind, P. Stone, A. Lacis, S. Lebedeff, R. Ruedy, and L. Travis, Efficient three-dimensional global models for climate studies: Models 1 and 2, *Mon. Wea. Rev.*, *111*, 609-662, 1983.
- Harnisch, J., R. Borchers, P. Fabian, and M. Maiss, Tropospheric trends of CF₄ and C₂F₆ since 1982 derived from SF₆ dated stratospheric air, *Geophys. Res. Lett.*, *23*, 1099, 1996.
- Hartke, G.J., and D. Rind, Improved Surface and Boundary layer models for the Goddard Institute for Space Studies general circulation model., *Jour. Geophys.*, *102*, 16407-16442, 1997.
- Hartley, D., and R. Prinn, Feasibility of determining surface emissions of trace gases using an inverse method in a three-dimensional chemical transport model, *J. Geophys. Res.*, *98*, 5183-5197, 1993.

- Heimann, M., Atmospheric Chemistry - Dynamics of the Carbon Cycle, , 375, 629-630, 1995.
- Heimann, M., and C. Keeling, A three-dimensional model of atmospheric CO₂ transport based on observed winds: 2. Model description and simulated tracer experiments. In: D.H. Peterson (Ed.), Aspects of Climate Variability in the Pacific and Western Americas, *Geophys. Monograph*, 55, 237-275, 305-363, 1989.
- Heimann, M., C.D. Keeling, and I.Y. Fung, Simulating the atmospheric carbon dioxide distribution with a three-dimensional tracer model. In J. R. Trabalka and D. E. Reichle, *The Changing Carbon Cycle: A Global Analysis*, 16-49, 1986.
- Houghton, J.T., L.G.M. Filho, B.A. Callandar, N. Harris, A. Kattenberg, and K. Maskell, *Climate Change 1995: Contribution of Working Group I to the Second Assessment Report of the Intergovernmental Panel on Climate Change.*, 572 pp., Climate Change 1995: The Science of Climate Change, Cambridge University Press, New York, 1995.
- Hurst, D.F., P.S. Bakwin, R.C. Myers, and J.W. Elkins, Behavior of trace gas mixing ratios on a very tall tower in North Carolina, *J. Geophys. Res.*, 102, 8825-8835, 1997.
- IGBP, A Synthesis of GCTE and Related Research, GCTE, Stockholm, 1997.
- Jacob, D.J., M.J. Prather, P.J. Rasch, R.L. Shia, and e. al, Evaluation and intercomparison of global atmospheric transport models using Rn-222 and other short-lived tracers, *J. of Geophysical Research--Atmospheres*, 102, 5953-5970, 1997.
- Jacob, D.J., M.J. Prather, S.C. Wofsy, and M.B. McElroy, Atmospheric distribution of 85Kr simulated with a general circulation model., *Jour. Geophys. Res.*, 92, 6614-6626, 1987.
- Kasibhatla, P.S., H.L. II, and W.J. Moxim, Global NO_x, HNO₃, PAN and NO distributions from fossil-fuel combustion emissions: A model study, *Jour. Geophys. Res.*, 98, 7165-7180, 1993.
- Keeling, C., T. Whorf, M. Wahlen, and J.v.d. Plicht, Interannual extremes in the rate of rise of atmospheric carbon dioxide since 1980, *Nature*, 375, 666-670, 1995.
- Keeling, W., Evaluation of Conservation Tillage Cropping Systems for Cotton on the Texas Southern High Plains, *J. of Prod. Agricul.*, 2, 269-273, 1989.
- Law, Simmons, and Bud, Applications of an atmospheric tracer model to the high southern latitudes, *Tellus*, 44B, 358-370, 1992.
- Law, R., P. Rayner, A. Denning, D. Erickson, I.Y. Fung, M. Heimann, S. Piper, M. Ramonet, S. T. Aguchi, J. Taylor, C. Trudinger, and I. Watterson, Variations in modeled atmospheric transport of carbon dioxide and the consequences for CO₂ inversions, *Global Biogeochem. Cycles*, 10, 783-796, 1996.
- Levin, I., and V. Hesshaimer, Refining of Atmospheric Transport Model Entries by the Globally Observed Passive Tracer Distributions of (85)Krypton and Sulfur Hexafluoride (SF₆), *J. of Geophysical Research--Atmospheres*, 101, 16745-16755, 1996.
- Levy, H., J.D. Mahlman, and W.J. Moxim, Tropospheric N₂O variability, *Journal of Geophysical Research*, 87, 3061-3080, 1982.
- Louis, J.F., A parametric model of vertical eddy fluxes in the atmosphere, *Boundary Layer Meteorol*, 17, 187-202, 1979.
- Mahlman, J.D., and S.E. Strahan, Evaluation of the skyhi general circulation model using aircraft N₂O measurements. Tracer variability and diabatic meridional circulation, *J. of Geophys. Res.-Atmos*, 99, 10319-10332, 1994.
- Mahlman, J.D., and L.J. Umscheid, Dynamics of the middle atmosphere: successes and problems of the GFDL "SKYHI" general circulation models, *Dynamics of the Middle Atmos.*, 501-525, 1984.
- Maiss, M., and I. Levin, Global Increase of SF₆ Observed in the Atmosphere, *Geophysical Research Letters*, 21, 569-572, 1994.
- Maiss, M., L.P. Steele, R.J. Francey, P.J. Fraser, and e. al, Sulfur Hexafluoride--A Powerful New Atmospheric Tracer, *Atmospheric Environment*, 30, 1621-1629, 1996.
- Marland, G., T.A. Boden, R.C. Griffith, S.F. Huang, P. Kanciruk, and T.R. Nelson, *Estimates of CO₂ emissions from fossil fuel burning and cement manufacturing, based on the U.S. Bureau of Mines cement manufacturing data*, , Carbon Dioxide Information Analysis Center, 1989.
- McFarlane, N.A., G.J. Boer, J.P. Blanchet, and M. Lazare, The Canadian Climate Centre second generation circulation model and its equilibrium climate, *Journal of Climate*, 5, 1013-1044, 1992.
- Nakazawa, T., K. Miyashita, S. Aoki, and M. Tanaka, Temporal and Spatial Variations of Upper Tropospheric and Lower Stratospheric Carbon Dioxide, *Tellus Series B-Chem. & Phys. Meteor.*, 43, 106-117, 1991.
- Patra, P.K., S. Lal, B.H. Subbaraya, C.H. Jackman, and P. Rajaratnam, Observed vertical profile of sulfur hexafluoride and its atmospheric applications, *Journal of Geophysical Research*, 102, 8855-8859, 1997.
- Plumb, R.A., and D.D. McConlogue, On the meridional structure of long-lived tropospheric constituents., *J. of Geophys. Res.*, 93, 15897-15913, 1988.

- Prather, M., Time scales in atmospheric chemistry- Theory, GWPS for CH₄ and CO, and Runaway Growth, *Geophys. Res. Letters*, 23, 2597-2600, 1996.
- Prather, M., M. McElroy, S. Wofsy, G. Russel, and D. Rind, Chemistry of the global troposphere: Fluorocarbons as tracers of air motion, *J. of Geophys. Res.*, 92, 186, 1987.
- Randall, D., P. Sellers, and J. Berry, A revised land surface parameterization (SiB2) for atmospheric GCMs. Part III: The greening of the Colorado State University General Circulation Model, *Journal of Climate*, 9, 738-763, 1996.
- Randall, D.A., and D.M. Pan, Implementation of the Arakawa-Schubert parameterization with a prognostic closure, *The Representation of Cumulus Convection in Numerical Models*, 137-144, 1993.
- Randall, D.A., Q. Shao, and C.H. Moeng, A second order bulk boundary layer model, *J. of Atmos. Sci.*, 49, 1903-1923, 1992.
- Ravishankara, A.R., S. Solomon, A.A. Turnispeed, and R.F. Warren, Atmospheric lifetimes of long-lived halogenated species, *Science*, 259, 194-199, 1993.
- Rayner, P., and R. Law, A comparison of modelled responses to prescribed CO₂ sources, CSIRO Division of Atmospheric Research, 1995.
- Russell, G., and J. Lerner, A new finite difference scheme for tracer transport equation, *J. of Appl. Meteor.*, 20, 1485-1498, 1981.
- Sellers, P., C. Tucker, G. Collatz, S. Los, C. Justice, D. Dazlick, and D. Randall, A revised land surface parameterization (SiB2) for atmospheric GCMs. Part II The generation of global fields of terrestrial biophysical parameters from satellite data, *Journal of Climate*, 9, 706-737, 1996.
- Suarez, M.J., A. Arakawa, and D.A. Randall, Parameterization of the planetary boundary layer in the UCLA general circulation model: Formulation and Results., *Mon. Wea. Rev.*, 111, 2224-2243, 1983.
- Taguchi, S., A three-dimensional model of atmospheric CO₂ transport based on analyzed winds: model description and simulation results for TRANSCOM, *Journal of Geophysical Research*, 101, 15099-15109, 1996.
- Tans, P., T. Conway, and T. Nakazawa, Latitudinal distribution of the sources and sinks of atmospheric carbon dioxide derived from surface observations and an atmospheric transport model, *J. Geophys. Res.*, 94, 5151-5172, 1989.
- Tans, P., I. Fung, and T. Takahashi, Observational constraints on the global atmospheric CO₂ budget, *Science*, 247, 1431-1438, 1990.
- Tiedke, M., A comprehensive mass flux scheme for cumulus parameterization in large-scale models., *Mon. Weather Rev.*, 117, 1779-1800, 1989.
- Tobler, W., Population database of the Consortium for International Earth Science Information Network (CIESIN) and the Environmental Systems research Institute, Inc. (ESRI), through the national Center for Geographic information and Analysis, University of California Department of Geography, Santa Barbara, 1995.
- United Nations, 1992 *Energy Statistics Yearbook*, , Department for Economic and Social Information and Policy Analysis, 1994.
- Vorosmarty, C.J., R. Wasson, and J. Richey, Modelling the Transport and Transformation of Terrestrial Materials to Freshwater and Coastal Ecosystems, IGBP, Stockholm, 1997.
- Weiss, W., A. Sittkus, H. Stockburger, and H. Sartorius, Large-scale atmospheric mixing derived from meridional profiles of Krypton 85, *J. Geophys. Res.*, 88, 8574-8578, 1983.
- Yaolin, S., and Z. Yuanqing, Some tectonic aspects of the Tibetan plateau, *Tectonophys.*, 219, 223-233, 1993.